Enhancement of spin-orbit interaction and the effect of interface diffusion in quaternary InGaAsP/InGaAs heterostructures

Makoto Kohda[1,2,*] and Junsaku Nitta[1]
[1]*Department of Materials Science, Tohoku University, 6-6-02 Aramaki-Aza Aoba, Aoba-ku, Sendai 980-8579, Japan*
[2]*PRESTO, Japan Science and Technology Agency, 4-1-8 Honcho, Kawaguchi, Saitama 332-0012, Japan*
(Received 3 September 2009; revised manuscript received 5 November 2009; published 15 March 2010)

The enhancement of spin-orbit interaction due to simultaneous control of both valence-band offset and electron probability density of the conduction band in a quaternary InGaAsP/InGaAs heterointerface is demonstrated. Weak antilocalization is measured to determine the strength of the Rashba spin-orbit interaction with different gate bias voltages and analyzed by quantum correction of the conductance developed by L. E. Golub [Phys. Rev. B **71**, 235310 (2005)]. The Rashba spin-orbit interaction parameter is increased up to $\alpha=10.4\times10^{-12}$ eV m with sheet carrier density $N_s=2\times10^{11}$ cm^{-2}. To confirm such a strong effective magnetic field by comparison with the Zeeman energy, we also measure weak antilocalization in the presence of the in-plane magnetic field. A weak antilocalization signal remains up to $B_{\parallel}=3.0$ T, resulting in direct evidence of strong spin-orbit interaction in the InGaAsP/InGaAs heterostructure. By taking the interface diffusion at the InGaAsP/InGaAs into account, the obtained Rashba spin-orbit interaction parameter α is found to be quantitatively consistent with theoretical calculation derived from the $k\cdot p$ theory.

DOI: 10.1103/PhysRevB.81.115118 PACS number(s): 71.70.Ej, 72.25.Rb, 73.20.Fz, 73.63.Hs

I. INTRODUCTION

Spin-orbit interaction (SOI) plays a significant role in the fundamental physics of spin-related phenomena[1–10] as well as in the realization of spin-based functionalities[11–16] in semiconductors. This is because the SOI provides a momentum-dependent effective magnetic field[2,3,17,18] and a spin-dependent orbital modulation for electrons.[4,14–16] Consequently, manipulating the SOI in semiconductor heterostructures has become an important prerequisite in spintronics. In semiconductor two-dimensional electron gas (2DEG), structure inversion asymmetry induces the Rashba SOI, and it can be controlled by the external gate bias.[2,3,10,19] This enables us to electrically control the spin precession without any external magnetic fields.[20,21] Recently, a mesoscopic Stern-Gerlach spin filter and spin current generation have been theoretically proposed with the utilization of the spatial- and time-dependent Rashba SOI, respectively.[22–24] These theoretical proposals reveal that the SOI plays a central role not only for electrical spin manipulation, but also for electrical spin generation and detection. Since the enhancement of the Rashba SOI parameter α as well as its carrier dependence $d\alpha/dN_s$ induces higher spin polarization for a Stern-Gerlach spin filter[22] and for spin currents,[23,24] the way to enhance the Rashba SOI has become a key issue in SOI-related semiconductor physics.

In 2DEGs, an internal electric field generating the Rashba SOI originates from the band bending inside a quantum well (QW) and the band offset at the heterointerface.[19] In addition, these two electric fields are weighted by the electron probability density inside the QW. It is also noteworthy that electric field contributions to the Rashba SOI originate from the *valence-band* structure, not from the *conduction band*, in the $k\cdot p$ theory.[17] In previous research, several groups have reported an enhanced Rashba SOI,[25,26] but only considered either the electron probability density at the heterointerface or band offset alignment in valence-band structure. One possible reason is that, in ternary-based heterostructures such as InAlAs/InGaAs as widely studied in SOI analysis, the compositional variation of group-III elements to design a band offset is limited due to the lattice relaxation above the critical thickness causing defect formation. As a result, it makes difficult to design a wide variety of band offsets to simultaneously control the valence-band offset and the electron probability density.

To overcome this obstacle, we propose quaternary-alloy-based heterostructures. $(In_{0.53}Ga_{0.47}As)_x(InP)_{1-x}/InGaAs$ is lattice matched to InP and also epitaxially grown on a strained InGaAs layer. Since both conduction- and valence-band offsets can be simultaneously controlled by changing the relative ratio between $In_{0.53}Ga_{0.47}As$ and InP, reduction of the conduction-band offset is possible for positioning higher electron probability density at the $(In_{0.53}Ga_{0.47}As)_x(InP)_{1-x}/InGaAs$ interface, and a relatively large valence-band offset remains due to a wide band gap of InP, expecting the enhancement of the Rashba SOI parameter α.

Although an atomically flat interface is prerequisite for the enhancement of the Rashba SOI to efficiently introduce the electric field at the heterointerface, it is difficult to achieve an ideal interface in $(In_{0.53}Ga_{0.47}As)_x(InP)_{1-x}/InGaAs$ because both group-III and group-V elements must be switched at the interface, resulting in compositional fluctuation due to interface diffusion.[27,28] Since elemental inhomogeneity dramatically reduces the electric field at the interface, the Rashba SOI is expected to be sensitive to the interface diffusion. However, to date, there has been no theoretical analysis of the Rashba SOI taking into account the effect of interface diffusion.

In the present work, we designed $(In_{0.53}Ga_{0.47}As)_{0.41}(InP)_{0.59}/In_yGa_{1-y}As$ based 2DEG structures and measured magnetoconductance to analyze weak antilocalization (WAL) with different gate bias voltages. It is shown that 10.4×10^{-12} eV m of the Rashba SOI parameter

 ©2010 The American Physical Society

TABLE I. Active layer structures of three different 2DEG samples. Layer sequence is listed from the sample surface to the buffer layer. Numbers1–3 show different quantum well thicknesses and In compositions in the $In_yGa_{1-y}As$ layer. Layer thickness is shown in units of nm.

	No. 1	No. 2	No. 3
$In_{0.52}Al_{0.48}As$	25	25	25
$(In_{0.52}Al_{0.48}As)_{0.3}(In_{0.53}Ga_{0.47}As)_{0.7}$	3	3	3
$In_yGa_{(1-y)}As$	10	5	10
	$y=0.53$	0.8	0.8
$(In_{0.53}Ga_{0.47}As)_{0.41}(InP)_{0.59}$	5	5	5
$In_{0.52}Al_{0.48}As$	15	15	15
n-$In_{0.52}Al_{0.48}As$ ($N_d=4\times10^{18}$ cm^{-3})	6	6	6
$In_{0.52}Al_{0.48}As$	200	200	200

α is achieved due to the enhanced interface contribution. In the theoretical calculation, we take the effect of interface diffusion into account and find that 1 nm compositional fluctuation dramatically reduces the Rashba SOI parameter α, which is quantitatively in good agreement with the experimental results.

II. THEORY OF RASHBA SPIN-ORBIT INTERACTION AND DESIGN OF HETEROINTERFACE

Layer structures of three different In compositions and QW thicknesses investigated here are summarized in Table I. Solid and dashed lines in Fig. 1 show the energy-band profile and electron probability density for a 10 nm $In_{0.8}Ga_{0.2}As$ QW structure under gate bias voltages of −4.5 and +2.5 V, respectively. According to the $k\cdot p$ perturbation theory, the Rashba SOI parameter α is described as follows:[19]

$$\alpha = \frac{\hbar^2 E_P}{6m_0}\vec{e}_z\left[\langle\Psi(z)|\Gamma_F|\Psi(z)\rangle + \sum_n \Gamma_{In}S_n|\Psi(z_n)|^2\right], \quad (1)$$

where

$$\Gamma_F = \left[\frac{1}{[E_F - E_{\Gamma7}^{QW}(z)]^2} - \frac{1}{[E_F - E_{\Gamma8}^{QW}(z)]^2}\right](1-\Theta)\varphi'(z) + \left[\frac{1}{[E_F - E_{\Gamma7}^{B}(z)]^2} - \frac{1}{[E_F - E_{\Gamma8}^{B}(z)]^2}\right]\Theta\varphi'(z), \quad (2)$$

$$\Gamma_{In} = \frac{\Delta E_{\Gamma7}}{2}\left[\frac{1}{[E_F - E_{\Gamma7}^{QW}(z_n)]^2} + \frac{1}{[E_F - E_{\Gamma7}^{B}(z_n)]^2}\right] - \frac{\Delta E_{\Gamma8}}{2}\left[\frac{1}{[E_F - E_{\Gamma8}^{QW}(z_n)]^2} + \frac{1}{[E_F - E_{\Gamma8}^{B}(z_n)]^2}\right]. \quad (3)$$

The first and second terms in Eq. (1) correspond to expectation values of the electric field inside the QW and at the heterointerface, respectively, and these two terms are categorized as the field contribution and the interface contribution of the Rashba SOI. Γ_F and Γ_{In} in Eq. (1) are determined by the band offsets and the band-gap energies in the valence and

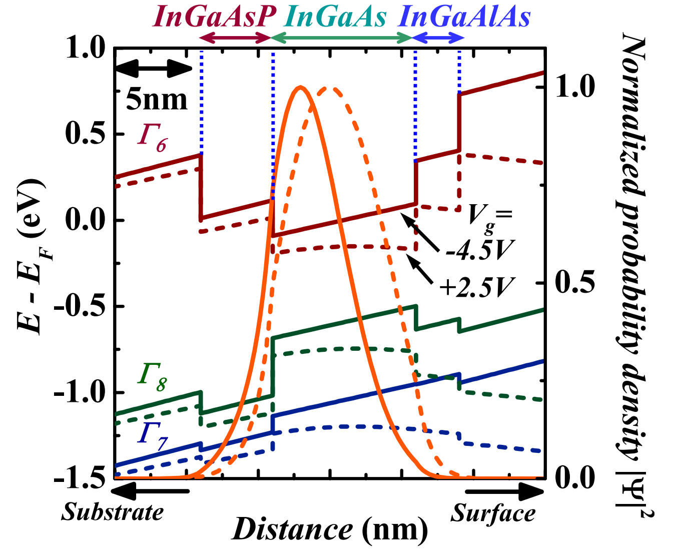

FIG. 1. (Color online) Energy-band profiles of conduction (Γ_6), valence (Γ_8), and spin split-off (Γ_7) bands in $In_{0.52}Al_{0.48}As$/5 nm $(In_{0.53}Ga_{0.47}As)_{0.41}(InP)_{0.59}$/10 nm $In_{0.8}Ga_{0.2}As$/3 nm $(In_{0.52}Al_{0.48}As)_{0.3}(In_{0.53}Ga_{0.47}As)_{0.7}$/$In_{0.52}Al_{0.48}As$ 2DEG structures calculated by the Poisson-Schrödinger equation. Each line correspond to Γ_6 (top), Γ_8 (middle), and Γ_7 (bottom) bands, respectively, whose energies are based on the position of Fermi energy E_F. Solid and dashed lines are the band structure under the gate bias voltage of $V_g=-4.5$ and +2.5 V, respectively. Normalized electron probability density $|\Psi|^2$ is also shown.

the spin split-off bands shown in Eqs. (2) and (3). In Eq. (1), z is the distance from the substrate, z_n is the position at the nth interface, E_p is the interband matrix element, $\hbar$ is the Planck's constant, m_0 is the free electron mass, e_z is the unit vector of z direction, and $\Psi(z)$ is the wave function for the confined electron in the conduction band. In Eqs. (2) and (3), E_F is the Fermi energy and $E_{\Gamma i}^{QW}(z)$ and $E_{\Gamma i}^{B}(z)$ $(i=7,8)$ are defined as the band-edge energies of the spin split-off $(i=7)$ and the valence bands $(i=8)$ in the QW and in the barrier layer. Γ_7 and Γ_8 denote the spin split-off band and the highest valence band. $\Delta E_{\Gamma7}$ and $\Delta E_{\Gamma8}$ are the band-offset energies of the spin split-off and valence bands between the QW and the barrier materials. Θ is the Heaviside step function, which is zero inside the QW and one, otherwise. $\varphi(z)$ is the macroscopic electric potential. From Eq. (1), one can understand that not only the field contribution but also the interface contribution plays an important role for the Rashba SOI. In an inverse high electron mobility transistor structure studied here, the electric fields both at the $(In_{0.53}Ga_{0.47}As)_{0.41}(InP)_{0.59}$/$In_{0.8}Ga_{0.2}As$ interface and inside the $In_{0.8}Ga_{0.2}As$ QW make additive contributions to the Rashba SOI due to the positive potential gradient as seen in the split-off and valence-band profiles in Fig. 1, and the sign of α becomes negative in Eq. (1), which is shown in the calculated and experimental results of α in Fig. 6. This is originated from the negative value of Γ_F and Γ_{In}. As a result, for efficiently introducing the interface contribution, the second term of Γ_{In} in Eq. (3) is maximized while the first term is minimized because of the subtractive contribution each other. $E_F - E_{\Gamma7}^{B}(z_n)$ and $E_F - E_{\Gamma8}^{B}(z_n)$ exhibit small contribu-

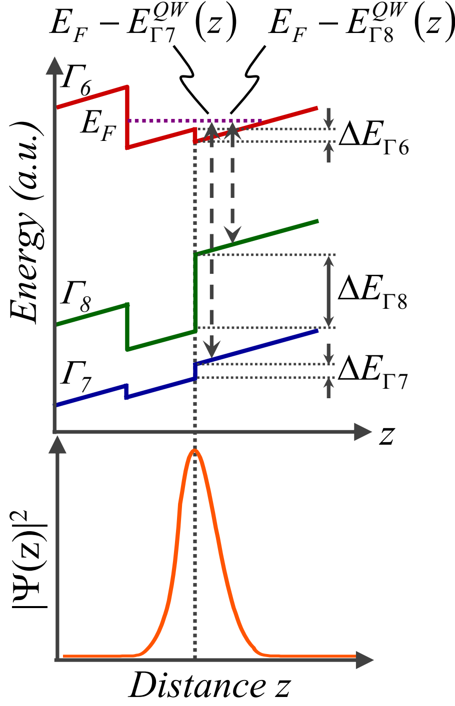

FIG. 2. (Color online) Schematic band structure and electron probability density for enhancing the interface contribution of Rashba SOI parameter. $\Delta E_{\Gamma 6}$, $\Delta E_{\Gamma 8}$, and $\Delta E_{\Gamma 7}$ are band offset energies of conduction, valence, and spin split-off bands at the interface, respectively. $E_F - E_{\Gamma 8}^{QW}(z_n)$ $[E_F - E_{\Gamma 7}^{QW}(z_n)]$ is the band-gap energy in a quantum well between Fermi level and valence band [spin split-off band].

tions to Eq. (3) since the band gap of the barrier is much larger than that of the QW. Therefore, for the enhancement of the Rashba SOI by taking advantage of the interface contribution, below criteria should be satisfied in Eqs. (1)–(3).

(1) The band offset in valence band ($\Delta E_{\Gamma 8}$) is maximized, while the band offset in spin split-off band ($\Delta E_{\Gamma 7}$) is minimized.

(2) In the QW, the band-gap energy between Fermi level and valence band $[E_F - E_{\Gamma 8}^{QW}(z)]$ is minimized, while the band-gap energy between Fermi level and spin split-off band $[E_F - E_{\Gamma 7}^{QW}(z)]$ is maximized.

(3) The conduction-band offset ($\Delta E_{\Gamma 6}$) is minimized.

(4) The electron probability density ($|\Psi(z_n)|^2$) at the interface is maximized.

A schematic band structure of ideal heterointerface satisfied the above criteria is shown in Fig. 2 with corresponding parameters. When we compare the band structure in Fig. 2 with the parameters in Eq. (3), criteria (1) and (2) minimize the first-term contribution, while the second term is maximized due to large $\Delta E_{\Gamma 8}$ and small $E_F - E_{\Gamma 8}^{QW}(z_n)$. In addition, the high electron probability density $|\Psi(z_n)|^2$ at the heterointerface enables us to enhance the second term in Eq. (1), which satisfies criteria (3) and (4). To bring the heterointerface design close to the ideal condition, a quaternary-alloy-based heterostructure $(In_{0.53}Ga_{0.47}As)_x(InP)_{1-x}/In_yGa_{1-y}As$ ($y=0.53$ or 0.8) becomes a possible candidate. In this heterointerface, both the conduction- and valence-band offsets can be widely controlled due to the large energy difference between $In_{0.53}Ga_{0.47}As$ (0.82 eV) and InP (1.42 eV) with the preservation of the lattice constant to the InP substrate. However, it should be noted that the valence, spin split-off, and conduction bands are simultaneously modified depending on the mutual composition in $(In_{0.53}Ga_{0.47}As)_x(InP)_{1-x}$. As a result, there is an optimal composition for the $(In_{0.53}Ga_{0.47}As)_x(InP)_{1-x}/In_yGa_{1-y}As$ interface. The ideal composition for maximizing the interface contribution corresponds to $x=0.41$ with $y=0.8$ in $(In_{0.53}Ga_{0.47}As)_x(InP)_{1-x}/In_yGa_{1-y}As$. At the $(In_{0.53}Ga_{0.47}As)_{0.41}(InP)_{0.59}/In_{0.8}Ga_{0.2}As$ interface in Fig. 1, a large valence-band offset of $\Delta E_{\Gamma 8}=0.333$ eV is achieved, while a small offset energy of $\Delta E_{\Gamma 7}=0.084$ eV is produced in the spin split-off band resulting in the large difference between the first and second terms in Eq. (3). In addition, the energy difference of 0.452 eV between the valence and the spin split-off bands in $In_{0.8}Ga_{0.2}As$ QW brings about much larger value of $E_F - E_{\Gamma 7}^{QW}(z_n)$ than $E_F - E_{\Gamma 8}^{QW}(z_n)$. These two conditions satisfy criteria (1) and (2) resulting in the increase in Γ_{In} in Eq. (1). When we consider the electron probability density inside the QW, a lowered conduction-band offset due to the reduced band gap of $(In_{0.53}Ga_{0.47}As)_{0.41}(InP)_{0.59}$ yields a higher probability density at the $(In_{0.53}Ga_{0.47}As)_{0.41}(InP)_{0.59}/In_{0.8}Ga_{0.2}As$ interface, which satisfies criteria (3) and (4). As a result, the enhancement of the interface contribution in Eq. (1) is expected.

III. SAMPLE STRUCTURES AND MEASUREMENT SETUP

Three sets of samples with different In compositions and thicknesses of $In_yGa_{1-y}As$ QW were grown on InP substrates by metal organic chemical vapor deposition as shown in Table I. We designed a 10 nm $In_{0.8}Ga_{0.2}As$ QW for the largest $d\alpha/dN_s$ and a 5 nm $In_{0.8}Ga_{0.2}As$ QW for the largest α based on the $k\cdot p$ perturbation theory. Since these two QWs are both lattice mismatched to the InP substrate, we also prepared a 10 nm $In_{0.53}Ga_{0.47}As$ lattice-matched QW for comparison of $In_{0.8}Ga_{0.2}As$ QWs. The epitaxial wafers were processed into 20×80 μm^2 Hall bar structures with Al_2O_3 or SiO_2 gate insulators/Au top contact. External magnetic field $B_\perp$ was applied perpendicular to the QW plane and the magnetoconductance was measured at different gate bias voltages to analyze the WAL at $T=0.3$ K. The Shubnikov-de Haas (SdH) oscillation and its temperature dependence were also measured for evaluating the sheet carrier density N_s, the electron mobility μ_e, and the effective mass m^*. The sheet carrier density modulated by the gate bias voltage showed 2.0 $(2.6)\times 10^{11}$ to 17.8 $(14.5)\times 10^{11}$ cm^{-2} and the corresponding elastic scattering length l_{tr} showed between 0.08 (0.07) and 2.1 (0.96) μm for $In_{0.8}Ga_{0.2}As$ ($In_{0.53}Ga_{0.47}As$) QW at $T=0.3$ K. From the amplitude variation of SdH oscillations between 1.6 and 60 K, the effective mass for $In_{0.8}Ga_{0.2}As$ ($In_{0.53}Ga_{0.47}As$) QW was deduced to 0.0408 (0.0439) under no gate bias voltage. For comparing Zeeman and SOI energies, while a constant in-plane magnetic field $B_\parallel$ was applied from 0.2 to 3.0 T, we measured the magnetoconductance by applying $B_\perp$ at $T=4.3$ K. Because of the limited

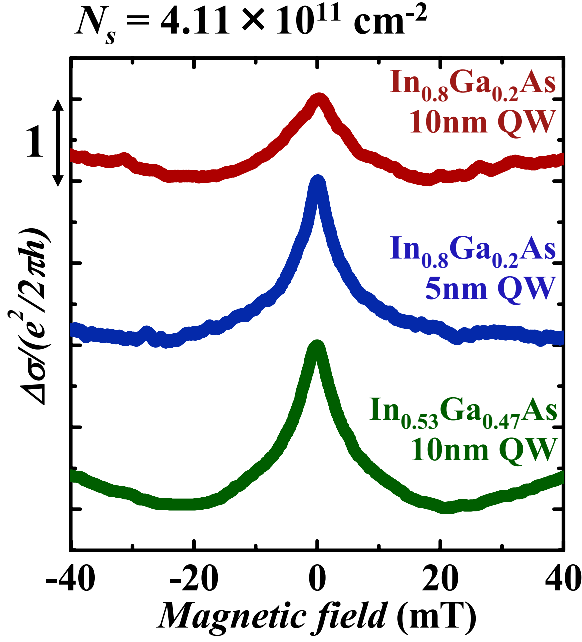

FIG. 3. (Color online) Measured magnetoconductances in 10 nm $In_{0.8}Ga_{0.2}As$, 5 nm $In_{0.8}Ga_{0.2}As$, and 10 nm $In_{0.53}Ga_{0.47}As$ QWs. Carrier densities between three samples are adjusted to N_s=4.11 $\times 10^{11}$ cm^{-2} by gate bias at T=0.3 K. Conductance is plotted in units of $e^2/2\pi h$.

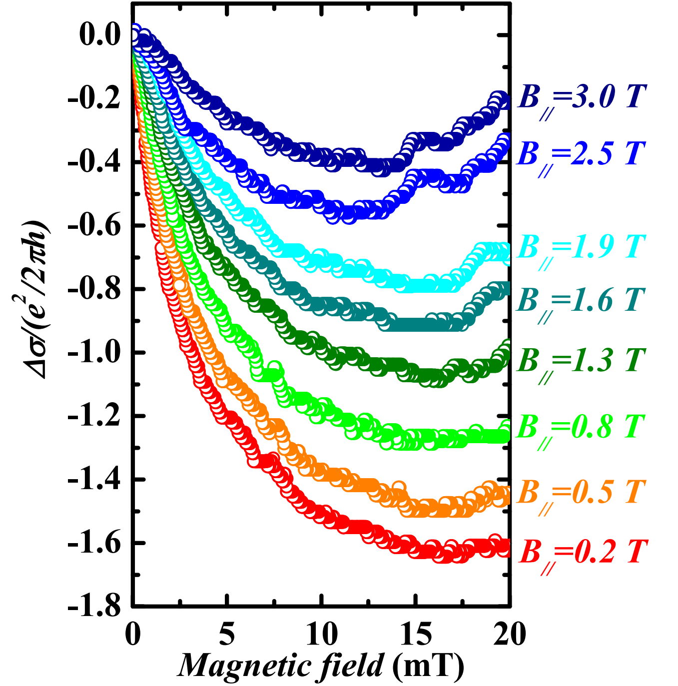

FIG. 4. (Color online) Perpendicular magnetic field dependence of conductance in 10 nm $In_{0.53}Ga_{0.47}As$ QW under different in-plane magnetic fields $B_{\parallel}$ from 0.2 to 3.0 T at T=4.3 K.

temperature control of the cryostat in the case of an in-plane magnetic field measurement, temperature conditions between the gate bias dependence and the application of an in-plane magnetic field on WAL measurements are different at 0.3 and 4.3 K. However, since the strength of the Rashba SOI is determined by the band-gap energy as shown in Eq. (1) and corresponding Rashba SOI parameters are virtually the same in 0.3 and 4.3 K, the temperature difference does not change the discussion for the presence of a strong SOI.

IV. WEAK ANTILOCALIZATION ANALYSIS

Figure 3 shows the WAL results in 10 nm $In_{0.8}Ga_{0.2}As$, 5 nm $In_{0.8}Ga_{0.2}As$, and 10 nm $In_{0.53}Ga_{0.47}As$ QWs at an adjusted carrier density of $N_s = 4.11 \times 10^{11}$ cm^{-2}. In all the QWs, the conductance peak is clearly observed at zero magnetic field, and negative magnetoconductance continues until $B_{\perp} = \pm 20$ mT. Since the observed negative magnetoconductance corresponds to the compensation of destructive interference for spin phase by the external magnetic field, broadening of negative magnetoconductance up to $B_{\perp} = \pm 20$ mT suggests the presence of a strong SOI. For obtaining direct evidence of such a strong effective magnetic field, we measured the WAL in the presence of the in-plane magnetic field $B_{\parallel}$. In small $B_{\parallel}$, the effective magnetic field induced by the SOI is still dominant, and the WAL is observed. However, in large $B_{\parallel}$, the Zeeman energy $g\mu_B B_{\parallel}$ forces the alignment of the electron spin along $B_{\parallel}$, and it suppresses the spin phase shift since electron spins precess in the same direction in the time-reversal symmetric path, resulting in the suppression of WAL. Accordingly, the strength of SOI can be evaluated by applying $B_{\parallel}$ through the variation from WAL to weak localization. Figure 4 shows the magnetoconductance with different values of $B_{\parallel}$ in the 10 nm $In_{0.53}Ga_{0.47}As$ QW at T =4.3 K. No gate bias voltage was applied in which the sheet carrier density showed 7.21×10^{11} cm^{-2}. We applied the $B_{\parallel}$ field with a superconducting coil magnet of ^{3}He cryostat, while a small coil magnet was used for the out-of-plane magnetic field. Due to the limited strength of $B_{\perp}$, we only measured the positive $B_{\perp}$ region. As $B_{\parallel}$ increased, the observed WAL was suppressed and positive magnetoconductance was observed in $B_{\perp} > +15$ mT. As explained above, this is because the electron spin was partially aligned to the $B_{\parallel}$ direction, in which the spin-relaxation time increases, leading to the suppression of WAL. In a previous study, Meijer *et al.* measured the effect of $B_{\parallel}$ on the WAL in InAlAs/InGaAs QWs.[29] In their structures, the WAL was completely suppressed after the application of $B_{\parallel}$=2.5 T due to the weak Rashba SOI parameter α of $\sim 4.3 \times 10^{-12}$ eV m. However, in the present QW structure, WAL was still observed in $B_{\parallel}$ =3.0 T, indicating the strong SOI induced by the $(In_{0.53}Ga_{0.47}As)_{0.41}(InP)_{0.59}/In_{0.53}Ga_{0.47}As$ heterostructure.

We then measured the magnetoconductance at various gate bias voltages to reveal the carrier density dependence of the Rashba SOI strength. Figures 5(a)–5(c) show gate bias dependences of WAL in 10 nm $In_{0.8}Ga_{0.2}As$, 5 nm $In_{0.8}Ga_{0.2}As$, and 10 nm $In_{0.53}Ga_{0.47}As$ QWs, respectively. As the gate bias increased to a positive value, positive magnetoconductance developed in $|B_{\perp}| > 10$ mT and the magnetic field where the conductance showed the minimum decreased, indicating the systematical change of the Rashba SOI. To quantitatively evaluate the strength of the Rashba SOI, we analyzed the experimental data with a quantum correction

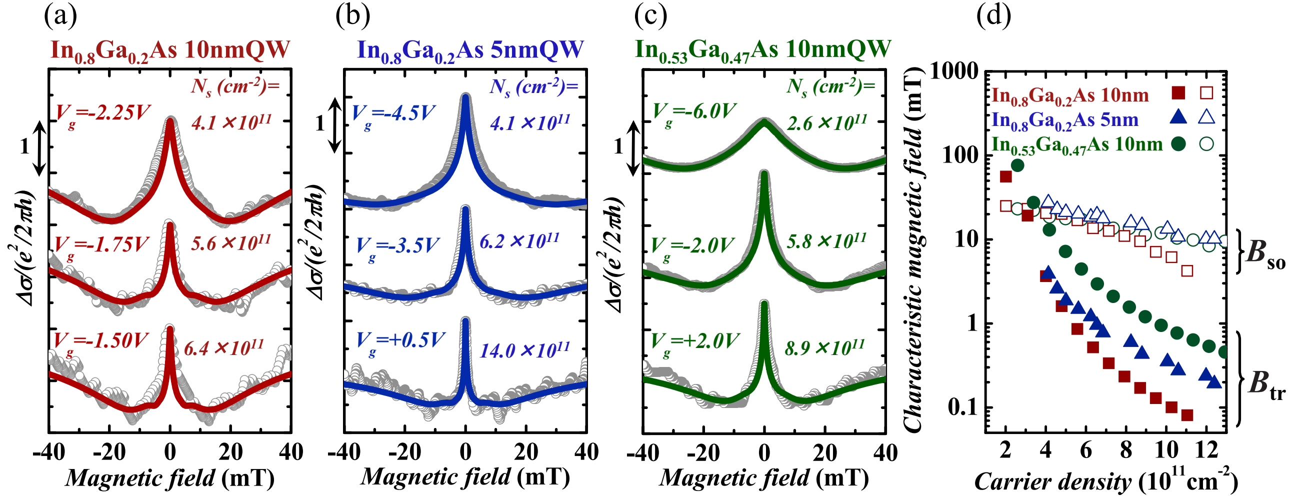

FIG. 5. (Color online) Experimental results (gray circles) of the quantum correction of the conductivity $\Delta\sigma$ in units of $e^2/2\pi h$ for (a) 10 nm $In_{0.8}Ga_{0.2}As$, (b) 5 nm $In_{0.8}Ga_{0.2}As$, and (c) 10 nm $In_{0.53}Ga_{0.47}As$ QWs with different gate bias voltages at $T=0.3$ K. The curves are offset for clarity. Corresponding carrier density N_s for the gate bias is also shown. The solid lines represent the best fits to the experimental results using the Golub theory (Ref. 31). (d) Carrier density dependence of transport magnetic field B_{tr} (closed symbols) and characteristic magnetic field of spin-relaxation length B_{so} (open symbols). B_{tr} is calculated from mean free path and B_{so} is derived from the ILP theory (Ref. 30).

model of the conductance.[30,31] Currently, two theoretical models are used for the WAL analysis, developed by Iordanskii, Lyanda-Geller, and Pikus (ILP) (Ref. 30) and that by Golub.[31] In the ILP theory, the model is applicable if the spin precession length is longer than the elastic scattering length, i.e., the characteristic field of spin precession length B_{so} should be smaller than the transport magnetic field $B_{tr} = \hbar/2el_{tr}^2$, where l_{tr} is the elastic scattering length. Accordingly, this model is limited to only weak SOI and/or low mobility 2DEG, so-called a diffusive regime. However, for utilizing the SOI in a ballistic regime such as the Stern-Gerlach spin filter, the fitting model for 2DEG structure with a strong SOI and/or a high electron mobility is of great importance, i.e., the Golub theory. To determine the appropriate theory for the WAL analysis, we plotted B_{tr} calculated from the elastic scattering length and $B_{so}=\hbar/4el_{so}^2$, where l_{so} is the spin-relaxation length, derived from the fitting by the ILP theory in Fig. 5(d). B_{tr} decreased over two orders of magnitude with increasing sheet carrier density, while B_{so} only decreased from 25 (23) to 4.2 (9.5) mT in the 10 nm $In_{0.8}Ga_{0.2}As$ ($In_{0.53}Ga_{0.47}As$) QW. This is because the electron mobility of the present 2DEGs is widely modulated by the gate bias from 0.78×10^4 to 11.6×10^4 cm^2/V s, while a strong SOI induces a short spin-relaxation length. As a result, most of the carrier density are in the ballistic regime, and we applied the Golub theory to extract the Rashba SOI parameter α. The conductivity correction due to WAL in the Golub theory[31] is given by a sum of two terms,

$$\sigma\left(B,\Omega\tau_{tr},\frac{\tau_{tr}}{\tau_\varphi}\right) = \sigma_a\left(B,\Omega\tau_{tr},\frac{\tau_{tr}}{\tau_\varphi}\right) + \sigma_b\left(B,\Omega\tau_{tr},\frac{\tau_{tr}}{\tau_\varphi}\right), \quad (4)$$

where σ_a and σ_b can be interpreted as the backscattering and nonbackscattering interference corrections to conductivity, respectively. Parameters for fitting the experimental data are the spin-orbit precession frequency Ω, the phase coherent time τ_φ, and the elastic scattering time τ_{tr}. τ_{tr} is obtained from the electron mobility $\mu_e=e\tau_{tr}/m^*m_0$, where e is the electron charge and m_0 is the free-electron mass, and one can derive τ_{tr} from the SdH measurement by evaluating the sheet resistance $R_s=1/eN_s\mu_e$ at zero magnetic field and by taking the fast Fourier transform of SdH oscillation for the sheet carrier density N_s. Then, we can reduce the fitting parameters into two, and Ω and τ_φ are extracted by the fitting of WAL. Indefinite summations are included in σ_a and σ_b terms, which determined the accuracy of the calculated value.[31] We continued the summation until the value for an addition being less than 10^{-11}. Since the spin splitting energy due to the SOI equals $2\hbar\Omega$, the Rashba SOI parameter is derived as $\alpha=\hbar\Omega/k_F$, where k_F is the Fermi wave vector. The calculated WAL curves are shown as solid lines in Figs. 5(a)–5(c). The calculated results are well fitted to the experimental curves, and we extracted the Rashba SOI parameter α for all experimental data. The closed circles in Figs. 6(a)–6(c) show the extracted α on the sheet carrier density N_s for three different QWs. Values of α reached 10.0×10^{-12} eV m in all structures when the carrier density decreases down to $N_s=2\times10^{11}-4\times10^{11}$ cm^{-2}. It is worth noting that $\alpha = 10.4\times10^{-12}$ eV m in the 10 nm $In_{0.8}Ga_{0.2}As$ QW corresponds to the equal value for the largest α reported in WAL measurements.[32] As can be seen in Fig. 1, the electron probability density is shifted to the $(In_{0.53}Ga_{0.47}As)_{0.41}(InP)_{0.59}/In_{0.8}Ga_{0.2}As$ interface under the negative bias condition, i.e., lower carrier density, resulting in the enhancement of the interface contribution.

The modulation sensitivity of α on the carrier density, $|d\alpha/dN_s|$, exhibits 6.1×10^{-28}, 4.3×10^{-28}, and 4.0×10^{-28} eV m^3 in 10 nm $In_{0.8}Ga_{0.2}As$, 5 nm $In_{0.8}Ga_{0.2}As$, and 10 nm $In_{0.53}Ga_{0.47}As$ QWs, respectively, where large $d\alpha/dN_s$'s are obtained in comparison with the 10 nm $In_{0.52}Al_{0.48}As/In_{0.8}Ga_{0.2}As$ 2DEG with no additional inter-

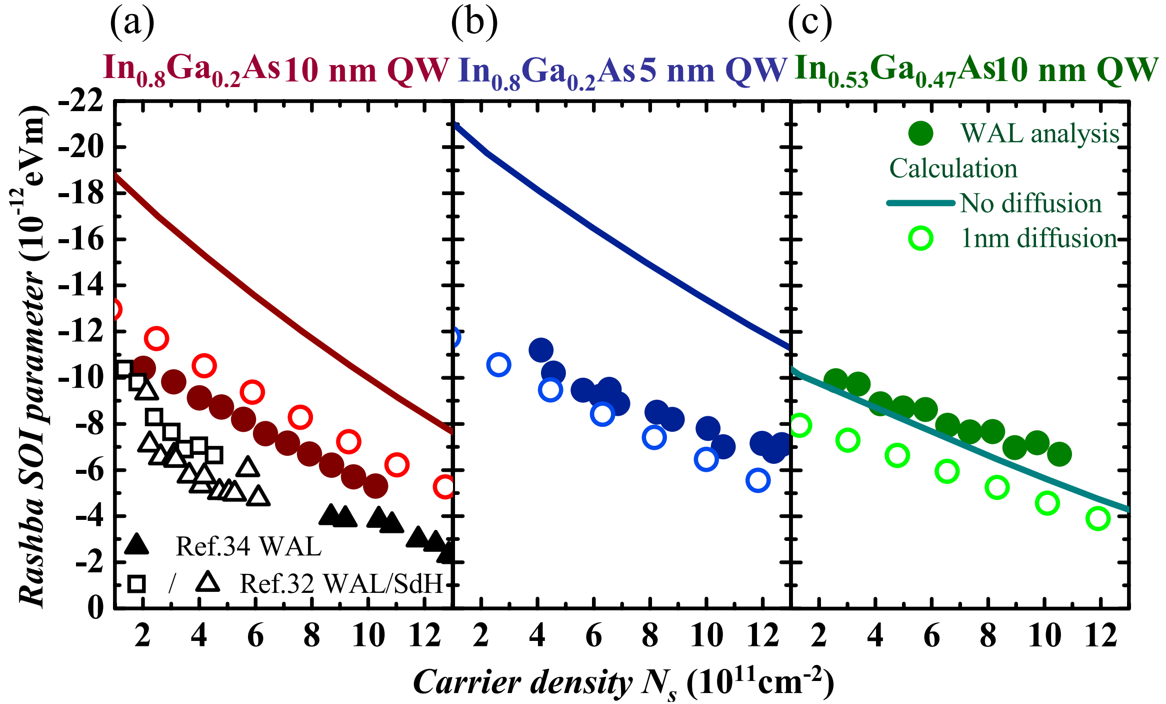

FIG. 6. (Color online) Carrier density dependence of the Rashba SOI parameter α by fitting the experimental results with the Golub theory (closed circles) and calculated results from the $k\cdot p$ theory (lines and open circles) for (a) 10 nm $In_{0.8}Ga_{0.2}As$, (b) 5 nm $In_{0.8}Ga_{0.2}As$, and (c) 10 nm $In_{0.53}Ga_{0.47}As$ QWs. Solid lines and open circles represent theoretical results with no interface diffusion and 1 nm interface diffusion at $(In_{0.53}Ga_{0.47}As)_{0.41}(InP)_{0.59}/In_yGa_{1-y}As$ heterostructure, respectively. Closed triangles are the results in $In_{0.52}Al_{0.48}As/In_{0.8}Ga_{0.2}As$ QW (Refs. 33 and 34). Open squares and triangles are $In_{0.53}Ga_{0.47}As/In_{0.77}Ga_{0.23}As$ QW which obtained the largest α and $d\alpha/dN_s$ in the WAL measurement (Ref. 32).

face as shown by the closed triangular plots in Fig. 6(a).[33,34] When we compare the same N_s region between 2×10^{11} and 6×10^{11} cm^{-2}, the observed $d\alpha/dN_s$ in the 10 nm $In_{0.8}Ga_{0.2}As$ QW is comparable to the largest $d\alpha/dN_s$ value obtained in the WAL analysis, where $|d\alpha/dN_s|=8.1\times10^{-28}$ eV m^3.[32] The narrow quantum well of the 5 nm $In_{0.8}Ga_{0.2}As$ 2DEG results in the stronger confinement of the electron wave function leading to the smaller $d\alpha/dN_s$. In contrast, the 10 nm $In_{0.8}Ga_{0.2}As$ QW shows the largest $d\alpha/dN_s$ because the electron wave function is widely shifted due to both the weaker confinement of 10 nm and the reduced conduction-band offset at the $(In_{0.53}Ga_{0.47}As)_{0.41}(InP)_{0.59}/In_{0.8}Ga_{0.2}As$ interface, leading to substantial change in the balance between the interface and field contributions of the Rashba SOI.

In order to quantitatively explain the strength and the carrier dependence of the Rashba SOI parameter α, theoretical calculations based on the $k\cdot p$ theory were performed by using Eq. (1), and calculated results are shown as solid lines in Fig. 6. While the experimentally obtained α in the 10 nm $In_{0.53}Ga_{0.47}As$ QW quantitatively shows good agreement with the calculated results, those in 5 and 10 nm $In_{0.8}Ga_{0.2}As$ QWs are drastically lower in comparison with the calculation.

To explain such a large difference between experiment and calculation in the Rashba SOI parameter for $In_{0.8}Ga_{0.2}As$ QWs, let us consider the interface diffusion and interfacial reactions[27,28] since, in the quaternary InGaAsP/InGaAs interface, different group-III and/or group-V elements as well as the group-III/group-V ratio should be changed during the epitaxial growth leading to compositional fluctuation at the interface. In the InGaAs/InP heterointerface, the replacement of P by several monolayers (ML) of As has been revealed through secondary ion mass spectrometry,[28] and compositional gradation has been observed at the interface by transmission electron microscopy (TEM).[35] These results indicate that interface diffusion and interfacial reactions in semiconductor heterostructures may occur during the growth and/or subsequent device processing steps. Furthermore, strain-induced interface diffusion has been theoretically analyzed in GaAs/AlAs (Ref. 36) and also experimentally observed in SiGe/Si.[37,38] Since the 2DEG structures studied here are grown with different group-V elements existing at the interface and also with the preservation of the lattice strain, we carried out high-resolution TEM for the $(In_{0.53}Ga_{0.47}As)_{0.41}(InP)_{0.59}/In_{0.8}Ga_{0.2}As$ interface analysis. TEM images revealed contrast gradation within ~4 ML at the $(In_{0.53}Ga_{0.47}As)_{0.41}(InP)_{0.59}/In_{0.8}Ga_{0.2}As$ boundary. Since the observed contrast is caused by the different average elemental mass of the $In_{0.8}Ga_{0.2}As$ layer containing P, it indicates the P diffusion at the interface during the growth. Consequently, we recalculated the Rashba SOI parameter α by taking into account the interface diffusion, in which we assumed linear compositional change from $(In_{0.53}Ga_{0.47}As)_{0.41}(InP)_{0.59}$ to $In_{0.8}Ga_{0.2}As$ within a 1 nm region (~4 ML) at the interface by adopting the results of the TEM observation. The calculated Rashba SOI parameters are shown as open circles in Figs. 6(a)–6(c). The calculated

results are drastically decreased in contrast to the ideal interface case and are quantitatively in good agreement with the experimental results. These evidences strongly suggest that 1 nm interface diffusion considerably degrades the strength of the Rashba SOI. Since the compositional change at the interface brings about continuous variation of the band-gap energy, the interface contribution of the Rashba SOI at $(In_{0.53}Ga_{0.47}As)_{0.41}(InP)_{0.59}/In_{0.8}Ga_{0.2}As$ turns into a field contribution in the first term of Eq. (1). The electric field induced by the field contribution is much weaker than that by the interface contribution, resulting in the reduction in α. Although the interface diffusion existed at the $(In_{0.53}Ga_{0.47}As)_{0.41}(InP)_{0.59}/In_{0.8}Ga_{0.2}As$ interface, the Rashba SOI parameter α reached the largest value reported in WAL measurements[32] by simultaneously designing the band offset at the heterointerface and the position of the electron probability density. It strongly suggests that heterostructure design becomes indispensable for realizing large α and $d\alpha/dN_s$ as well as for device applications utilizing SOI. It also notes that further optimization of the growth condition to reduce the interface diffusion increases the Rashba SOI parameter.

While we can quantitatively explain the experimental α for $In_{0.8}Ga_{0.2}As$ QWs in terms of the interface diffusion, in the case of $In_{0.53}Ga_{0.47}As$ QW, it causes a further decrease in α as shown by the open circles in Fig. 6(c). One possible reason might be the enhanced diffusion in the strained $In_{0.8}Ga_{0.2}As$ QW. It has been reported that lattice strain enhances the interface diffusion in order to reduce the additional energy accumulated in the strained layer.[36] In addition, impurity diffusion is influenced by lattice defects such as vacancies and interstitials.[39] Since lattice strain can strongly affect the crystal defect density, it will change the diffusivity during the interface diffusion between lattice-matched and lattice-mismatched heterostructures. As a result, the lattice-matched $In_{0.53}Ga_{0.47}As$ QW is less affected by the interface diffusion. It is also noteworthy that the reduction in the calculated Rashba SOI parameter α due to 1 nm interface diffusion is less pronounced for the 10 nm $In_{0.53}Ga_{0.47}As$ QW in comparison with that for $In_{0.8}Ga_{0.2}As$ QWs. This is because the larger band gap of $In_{0.53}Ga_{0.47}As$ QW reduces the valence-band and split-off band offsets at the $(In_{0.53}Ga_{0.47}As)_{0.41}(InP)_{0.59}/In_{0.53}Ga_{0.47}As$ interface, resulting in a smaller interface contribution to the entire Rashba SOI.

V. CONCLUSION

We demonstrated the enhancement of the Rashba SOI due to the simultaneous control of both the valence-band offset and electron probability density of the conduction band in $(In_{0.53}Ga_{0.47}As)_{0.41}(InP)_{0.59}/In_yGa_{1-y}As$ based 2DEG structures. Comparison between the Rashba SOI and Zeeman coupling by the application of a static in-plane magnetic field $B_{\parallel}$ showed that WAL remained even in the application of $B_{\parallel}=3.0$ T, which revealed the existence of a strong SOI. By applying the Golub theory for the WAL analysis, the extracted Rashba SOI parameter α reached 10.0 $\times 10^{-12}$ eV m in all structures and showed $\alpha=10.4 \times 10^{-12}$ eV m in the 10 nm $In_{0.8}Ga_{0.2}As$ QW corresponding to the equal value for the largest α reported in the WAL analysis. Since the 2DEGs studied here were grown with different group-V elements and also with lattice strain, we carried out high-resolution TEM for interface analysis and revealed the presence of interface diffusion at $(In_{0.53}Ga_{0.47}As)_{0.41}(InP)_{0.59}/In_{0.8}Ga_{0.2}As$. After the recalculation of α taking into account the interface diffusion, we found that 1 nm interface diffusion considerably degraded the strength of the Rashba SOI, which quantitatively explains the experimental results obtained in 5 and 10 nm $In_{0.8}Ga_{0.2}As$ QWs.

ACKNOWLEDGMENTS

This work was partly supported by Grants-in-Aids from JSPS, MEXT, and SCOPE. Also this work was partly supported by Global COE Program "Materials Integration, Tohoku University." M.K. acknowledges support of the Sumitomo Foundation and the Mayekawa Foundation. J.N. acknowledges support of the Mitsubishi Foundation. This work was partly carried out at the Laboratory for Nanoelectronics and Spintronics, Research Institute of Electrical Communication, Tohoku University.

*makoto@material.tohoku.ac.jp

[1] M. I. D'yakonov and V. I. Perel', Sov. Phys. JETP **33**, 1053 (1971).
[2] J. Nitta, T. Akazaki, H. Takayanagi, and T. Enoki, Phys. Rev. Lett. **78**, 1335 (1997).
[3] G. Engels, J. Lange, Th. Schäpers, and H. Lüth, Phys. Rev. B **55**, R1958 (1997).
[4] S. Murakami, N. Nagaosa, and S. C. Zhang, Science **301**, 1348 (2003).
[5] Th. Schäpers, J. Knobbe, and V. A. Guzenko, Phys. Rev. B **69**, 235323 (2004).
[6] R. Winkler, Phys. Rev. B **69**, 045317 (2004).
[7] B. Andrei Bernevig, J. Orenstein, and Shou-Cheng Zhang, Phys. Rev. Lett. **97**, 236601 (2006).
[8] Th. Schäpers, V. A. Guzenko, M. G. Pala, U. Zülicke, M. Governale, J. Knobbe, and H. Hardtdegen, Phys. Rev. B **74**, 081301(R) (2006).
[9] M. Scheid, M. Kohda, Y. Kunihashi, K. Richter, and J. Nitta, Phys. Rev. Lett. **101**, 266401 (2008).
[10] Y. Kunihashi, M. Kohda, and J. Nitta, Phys. Rev. Lett. **102**, 226601 (2009).
[11] S. Datta and B. Das, Appl. Phys. Lett. **56**, 665 (1990).
[12] J. Nitta, F. E. Meijer, and H. Takayanagi, Appl. Phys. Lett. **75**, 695 (1999).
[13] S. D. Ganichev, E. L. Ivchenko, V. V. Bel'kov, S. A. Tarasenko, M. Sollinger, D. Weiss, W. Wegscheider, and W. Prettl, Nature (London) **417**, 153 (2002).
[14] Y. K. Kato, R. C. Myers, A. C. Gossard, and D. D. Awschalom,

Phys. Rev. Lett. **93**, 176601 (2004).
[15] Y. K. Kato, R. C. Myers, A. C. Gossard, and D. D. Awschalom, Science **306**, 1910 (2004).
[16] J. Wunderlich, B. Kaestner, J. Sinova, and T. Jungwirth, Phys. Rev. Lett. **94**, 047204 (2005).
[17] R. Winkler, *Spin-Orbit Coupling Effects in Two-Dimensional Electron and Hole Systems* (Springer, New York, 2003).
[18] M. Kohda, T. Bergsten, and J. Nitta, J. Phys. Soc. Jpn. **77**, 031008 (2008).
[19] Th. Schäpers, G. Engels, J. Lange, Th. Klocke, M. Hollfelder, and H. Lüth, J. Appl. Phys. **83**, 4324 (1998).
[20] T. Bergsten, T. Kobayashi, Y. Sekine, and J. Nitta, Phys. Rev. Lett. **97**, 196803 (2006).
[21] T. Koga, Y. Sekine, and J. Nitta, Phys. Rev. B **74**, 041302(R) (2006).
[22] J. Ohe, M. Yamamoto, T. Ohtsuki, and J. Nitta, Phys. Rev. B **72**, 041308(R) (2005).
[23] A. G. Mal'shukov, C. S. Tang, C. S. Chu, and K. A. Chao, Phys. Rev. B **68**, 233307 (2003).
[24] C. S. Tang, A. G. Mal'shukov, and K. A. Chao, Phys. Rev. B **71**, 195314 (2005).
[25] D. Grundler, Phys. Rev. Lett. **84**, 6074 (2000).
[26] Y. Lin, T. Koga, and J. Nitta, Phys. Rev. B **71**, 045328 (2005).
[27] D. C. Law, Y. Sun, C. H. Li, S. B. Visbeck, G. Chen, and R. F. Hicks, Phys. Rev. B **66**, 045314 (2002).
[28] P. E. Smith, S. H. Goss, S. T. Bradley, M. K. Hudait, Y. Lin, S. A. Ringel, and L. J. Brillson, J. Vac. Sci. Technol. B **22**, 554 (2004).
[29] F. E. Meijer, A. F. Morpurgo, T. M. Klapwijk, and J. Nitta, Phys. Rev. Lett. **94**, 186805 (2005).
[30] S. V. Iordanskii, Yu B. Lyanda-Geller, and G. E. Pikus, JETP Lett. **60**, 206 (1994).
[31] L. E. Golub, Phys. Rev. B **71**, 235310 (2005).
[32] V. A. Guzenko, Th. Schäpers, and H. Hardtdegen, Phys. Rev. B **76**, 165301 (2007).
[33] M. Kohda, T. Nihei, and J. Nitta, Physica E **40**, 1194 (2008).
[34] J. Nitta, T. Bergsten, Y. Kunihashi, and M. Kohda, J. Appl. Phys. **105**, 122402 (2009).
[35] J. Decobert and G. Patriarche, J. Appl. Phys. **92**, 5749 (2002).
[36] R. G. Dandrea and C. B. Duke, Phys. Rev. B **45**, 14065 (1992).
[37] S. S. Iyer and F. K. LeGoues, J. Appl. Phys. **65**, 4693 (1989).
[38] J.-M. Baribeau, R. Pascual, and S. Saimoto, Appl. Phys. Lett. **57**, 1502 (1990).
[39] Y. C. Chen, J. Singh, and P. K. Bhattacharya, J. Appl. Phys. **74**, 3800 (1993).